AIChE

Release of Dissolved Organic Matter from Melting Ice

Shuang Xue, Jing Chen, and Mei Tie

School of Environmental Science, Liaoning University, Shenyang 110036, China; Tiemei05@sohu.com (for correspondence)

Published online 26 February 2016 in Wiley Online Library (wileyonlinelibrary.com). DOI 10.1002/ep.12341

The elution behavior of dissolved organic matter (DOM) from melting ice, as well as the effect of freezing and thawing temperatures on the elution behavior of DOM from melting ice, was evaluated. DOM was fractionated using XAD resins into five fractions: hydrophobic acid (HPO-A), hydrophobic neutral (HPO-N), transphilic acid (TPI-A), transphilic neutral (TPI-N) and hydrophilic fraction (HPI). The bulk DOM and its five fractions, as well as ultraviolet (UV)-absorbing substances, trihalomethane (THM) and haloacetronitrile (HAA) precursors, and fluorescent materials in DOM exhibited a first flush behavior during ice melting, i.e., preferential elution with the early melt water fractions; the first flush behavior of DOM was stronger at higher freezing temperatures and/or at lower thawing temperatures, whereas DOM was eluted from the ice more uniformly at lower freezing temperatures and/or at higher thawing temperatures. The higher dissolved organic carbon (DOC) concentration in ice was, the higher degree of enrichments of DOM within the first melt water fraction was. HAA precursors were more strongly enriched in the early melt water samples than THM precursors during ice melting. The fluorescent materials were released more uniformly over the entire melt period, as compared with the bulk DOM. © 2016 American Institute of Chemical Engineers Environ Prog, 35: 1458–1467, 2016

Keywords: dissolved organic matter, ice melting, UV, fluorescence, chlorine reactivity

INTRODUCTION

Surface waters in regions of middle and high latitudes are usually ice-covered for several months. The contaminants in water will remain in ice cover that acts as a temporary storage medium during the freezing in winter, and then be released to water during the thawing in spring [1]. The amplification of contaminants during snowmelt has been well documented and is believed to can result in a pulse exposure to contaminants in aquatic ecosystems during early spring [2–5]. Brinmblecombe *et al*. [6,7] investigated the elution phenomena of ions from the artificially made ices during thawing, and reported that ion rich solution was preferentially obtained from the initial 20∼30% of melt. Li *et al*. [1] examined the discharge of nitrobenzene in ice during the thawing process. However, to the authors' knowledge no research has been undertaken to investigate the elution behavior of dissolved organic matter (DOM) in ice during thawing. DOM is a complex heterogeneous mixture composed of humic acids, fulvic acids, low molecular weight (MW) organic acids, carbohydrates, proteins, and other compound classes [8]. The nature and properties of DOM are of growing research interest because it can cause aesthetic concerns such as color, taste, and odor; lead to the binding and transport of organic and inorganic contaminants; provide sources and sinks for carbon [9–11]. Moreover, DOM acts as important precursor of disinfection by-products (DBPs) during water disinfection [12–14]. Knowledge on the release of DOM from melting ice is essential to understand their distribution, transport and fate in aquatic ecosystems in the spring melt period. Therefore, the goal of work described here was to examine the elution behavior of DOM from melting ice. Specific objectives included investigating the changes in concentrations and characteristics of DOM and its fractions released from melting ice, as well as evaluating the effect of freezing and thawing temperatures, the shape of ice block, and the thawing manner on the elution behavior of DOM from melting ice.

MATERIALS AND METHODS

Sample Collection and Preservation

Water samples for this study were collected from the Weigonghe River (WR) and the Dahuofang Resevior (DR) on 15 and 16 October 2013, respectively. WR and DR were selected because they are two distinct and different surface water systems, and therefore, differ in water quality characteristics. The majority of WR flow is made up of effluents from the North Wastewater Treatment Plant (NWTP); therefore, this sample was categorized as having significant anthropogenic impact. This NWTP, with a treatment capacity of 2×10^5 m^3/d, uses activated sludge process prior to discharge. DR, the largest reservoir with a maximum capacity of 2.2×10^7 m^3 in Liaoning province, is located at the midstream of the Hunhe River, 68 km northeast of Shenyang. This reservoir is the main source of drinking water production for the population of Shenyang and Fushun. WR runs through the city of Shenyang, with a length of 8.7 km. DR is categorized as water samples that have minimal anthropogenic (e.g., wastewater) impact. The characteristics of the WR and DR water samples were summarized in Table 1.

DOM Fractionation

DOM was fractionated into five classes: hydrophobic acid (HPO-A), hydrophobic neutral (HPO-N), transphilic acid (TPIA), transphilic neutral (TPI-N), and hydrophilic fraction (HPI), using XAD-8/XAD-4 resin chromatography. The isolation methods were described in detail by Xue *et al*. [15].

Table 1. Characteristics of WR and DR water samples.

Parameters	WR	DR
pH	7.6	7.3
TOC (mg/L)	8.9	1.9
DOC (mg/L)	7.2	1.6
UV-254 (cm^{-1})	0.126	0.039
Conductivity (μs/cm)	479.8	223.8
Turbidity (NTU)	9.7	4.1

Thawing Experiments

The feed water samples used in thawing experiments were WR and DR water samples. DR was adjusted to the same conductivity as WR. There were four sets of thawing experiments conducted on both WR and DR to investigate the effect of freezing and thawing temperatures on the elution behavior of DOM from melting ice in this study, designated as A, B, C, D, respectively. The freezing and thawing temperatures set for A, B, C, D sets of experiments were −15°C and 5°C, −25°C and 5°C, −15°C and 15°C, and −25°C and 15°C, respectively. In each set of thawing experiments, four 1.8-L sub-samples of each feed water sample set in a cylindrical container with inner diameter 10 cm and height 30 cm were frozen in a refrigerator, and then thawed in an environmental climate box. During thawing, the ice melt water were taken out from the cylindrical container at scheduled intervals (24h for A and B sets, and 6h for C and D sets, respectively) to determine the volume, dissolved organic carbon (DOC), absorbance of ultraviolet light at 254 nm (UV-254), trihalomethane formation potential (THMFP), haloacetronitrile formation potential (HAAFP), and fluorescence spectra of the liquid phase.

In addition, there were E and F sets of thawing experiments to study the effect of the shape of ice block and the thawing manner on the elution behavior of DOC during ice melting, by comparing the results of E and F sets of thawing experiments to those of A set, respectively. The freezing and thawing temperatures set for both E and F sets of experiments were −15°C and 5°C, respectively. In the E set of experiments, the containers of water samples were cuboid (length × width × height = 20cm × 20cm × 7 cm). In the F set of experiments, polystyrene insulations were applied at bottom and outer surface of the cylindrical containers with inner diameter 10 cm and height 30 cm so that heat transfer during freezing and thawing mainly occurred unidirectional (axially from top to bottom). This unidirectional downward freezing and thawing manner was similar to the natural freezing and thawing occurring in waters during winter and early spring.

The thawing experiments were also conducted on five DOM fractions isolated from WR. HPO-A, HPO-N, TPI-A, and TPI-N were adjusted to the same values of DOC and conductivity as HPI. These DOM fraction samples were frozen at −15°C, and then thawed at 15°C.

Analysis

DOC was analyzed using a Shimadzu TOC-5000 Total Organic Carbon Analyzer with auto-sampler. UV-254 was measured with a Cary 50 ultraviolet-visible (UV/Vis) spectrophotometer at 254 nm using a quartz cell with a 1-cm pathlength. The instrument was zeroed using Milli-Q water as a blank. Specific ultraviolet light absorbance (SUVA) was calculated as (UV-254/DOC) × 100.

THMFP and HAAFP measurements were performed according to Standard Method 5710B. The chlorine dosage for each water sample was determined such that a final residual chlorine of 3∼5 mg/L remained in the sample after the 7 days of incubation at 25°C. All samples were adjusted to a pH of 7 ± 0.2 using H_2SO_4 and NaOH. The neutralized solution was then buffered with a phosphate solution prior to incubation in amber bottles at 25 ± 2°C for 7 days. At the end of the incubation period, samples were dechlorinated using sodium sulfite (Na_2SO_3). Trihalomethanes (THMs) were extracted with methyl-tert butyl ether (MTBE) from the chlorinated samples using a modified EPA method 551.1. Five species of haloacetronitriles (HAAs), i.e. monochloroacetic acid (MCAA), dichloroacetic acid (DCAA), trichloroacetic acid (TCAA), monobromoacetic acid (MBAA), and dibromoacetic acid (DBAA), were analyzed in accordance with EPA method 552.2. MTBE was used as the sole extracting solvent. The concentrations of THMs and HAAs were measured using a gas chromatograph (CP-3800) with an electron capture detector (ECD).

Fluorescence spectra were obtained with a JASCO FP-6500 spectrofluorometer. The spectrofluorometer used a Xenon excitation source, and slits were set to 5 nm for both excitation and emission. Filtered water extracts were diluted to 1 mg/L of DOC with 0.01 mol/L potassium chlorate (KCl). The emission (Em) wavelength range was fixed from 290 to 550 nm (1-nm intervals), whereas the excitation (Ex) wavelength was increased from 220 to 400 nm (5-nm intervals). Scan speed was set at 1000 nm/min, generating an EEM in about 15 min. Blank sample (0.01 mol/L KCl) fluorescence was subtracted from all spectra. To eliminate the Rayleigh scattering interference in EEMs, the intensity values at points where the emission wavelength was the same as or twice the excitation wavelength, as well as those adjacent to them (±10 nm emission wavelength at the same excitation wavelength), were excised from the scan data and the excised values were replaced with zero [16]. In addition, this procedure was also applied to the data points in EMMs with an emission wavelength < the excitation wavelength or > twice the excitation wavelength. All data points whose value had been replaced with zero were excluded when calculating projected excitation-emission area in quantitative analyses of EEM spectra by means of the fluorescence regional integration (FRI) technique proposed by Chen *et al.* [17].

RESULTS AND DISCUSSION

Release of DOC

A concentration level of DOM during the melt process of ice was described by the concentration factor (CF) in this study, which is defined as the ratio between the DOM concentration of melt water obtained during the melt process of the ice sample and that of the original feed water corresponding to this ice sample in freeze-thaw treatments. The CF values of DOC during the melting of ice were plotted as a function of cumulative thawing ratio in Figure 1. The cumulative thawing ratio is determined as the ratio of the sum of volume of all melt water obtained before the sampling time to the original feed water.

As shown in Table 1, DOC of WR and DR were 7.2 mg/L and 1.6 mg/L, respectively. It could be found from the A∼D sets of thawing experiments conducted on both WR and DR that CF_{DOC} exhibited high values during the initial melting of ice, while the CF_{DOC} values were very low at the end of the melt period (Figure 1). As a result, 32.0∼63.2% of DOC in both WR and DR were released with the first 21.9∼26.5% of the melt water. The results indicated that DOM in ice was discharged in greatly elevated concentrations at an early stage of melting.

The first flush behavior of ions and dissolved organic chemicals from the natural snow and the artificially made ices during the melt, namely their enrichment in early melt water fractions, were already reported by several researchers

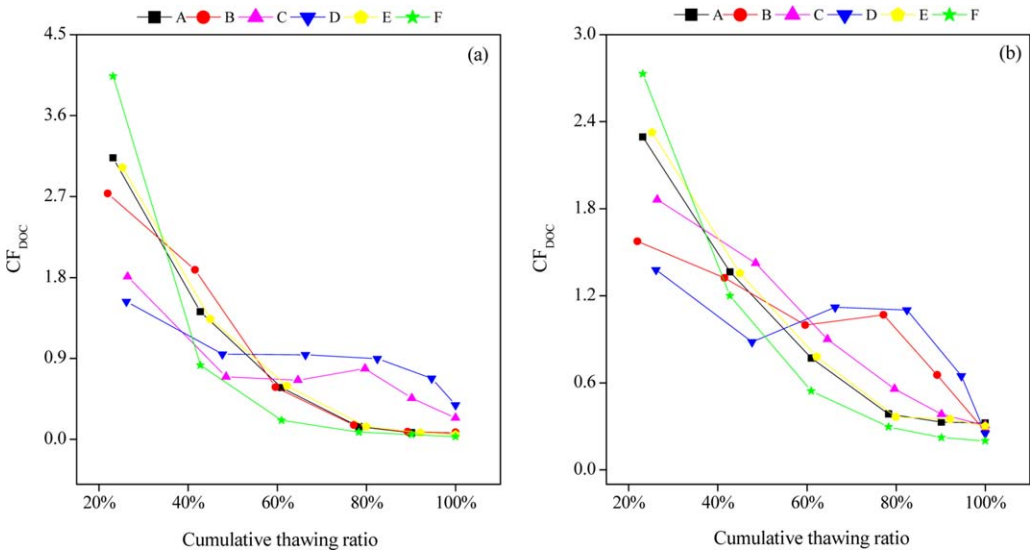

Figure 1. CF_{DOC} for (a) WR and (b) DR as a function of cumulative thawing ratio during ice melting. [Color figure can be viewed in the online issue, which is available at **wileyonlinelibrary.com**.]

[4,18–23]. This early release is attributed to a freezing-out of chemicals and small particles from the ice lattice during snow metamorphism occurring prior to snowmelt or ice formation [4]. When water congeals into ice, all water molecules will combine into a huge molecule [23]. In the structure of ice, each oxygen atom connects with four hydrogen atoms so as to form a tetrahedron, and each hydrogen atom connects with two oxygen atoms, in which closer hydrogen combines with oxygen by covalent bond, and farther hydrogen combines with oxygen by hydrogen bond [23–25]. The intensity of hydrogen bond is strong with a directionality, which can make each molecule arrange and combine according to a certain direction, so as to form a structure of tetrahedron. The structure of ice is arranged orderly by such a tetrahedral structure [26]. There are only four molecules around each water molecule, so many "holes" in the ice cannot be closely packed with water molecule like water. When ice melts into water, the tetrahedral structure of such five molecules of ice will break up gradually with the continuous supply of energy outside [24–26]. Knight [27] believed that the melt of ice crystal mainly depends on the initial type of crystal, and he summarized the melt of ice crystal into two kinds of basic mode: one is the melt of columnar ice crystal, the surface of ice crystal melts evenly at initial stage, and then a water layer with uneven thickness appears, one or two obvious bubbles are formed in column core, and then melting water tends to turn into one or several water drops having the minimum surface area; the other is the melt of flat-shaped ice crystal, its melting water doesn't shrink into a single water drop, but instead of a smooth round face totally covering the board. It was reported that the ice formed in the laboratory is a typical columnar ice structure [1]. During the freezing process, the pollutant fails to combine with the crystal lattice of ice, but instead of existing in the gap of ice [28]. During the melting process, ice begins to melt uniformly on the surface, later it will gradually form a water layer with inconsistent thickness and then form water drops [1,27]. When ice melts further, the pollutants in the gap of ice melt faster than crystal lattice of ice, and they are released rapidly into the water drops [1]. Meanwhile, during the freezing process, bubbles appear in the ice. The bubbles in the ice will absorb the pollutants [25,26]. The specific surface area of bubbles is large, which can make bubbles expose as the melt during the melting process, and make the pollutant molecules around the bubbles release, thus leading to higher amount of pollutants released from ice during the initial stage of ice melting [3,4]. On the other hand, there were a small portion of chemicals incorporated within the ice lattice of the ice grains during freezing, which were gradually released at late stage of melting [4]. Nakagawa *et al.* [29] also suggested that the concentration phenomenon occurs at an early stage of melting was induced by solute elution from the frozen phase to melt droplets that appeared on the thawing matrix. Meyer and Wania [4] believed that different organic chemicals will become dissolved in the melt water at different times during the melt process, and differential elution of organic compounds from a melting snow/ice may be related to differences in the compounds' distribution constants between the ice grain surface and the melt water.

As shown in Figure 1a, the highest CF_{DOC} values in the A, B, C, D sets of thawing experiments conducted on WR were 3.13, 2.73, 1.81, 1.53, respectively, while the lowest values were 0.06, 0.08, 0.23, 0.39, respectively. Similarly, the highest CF_{DOC} values of 2.29, 1.58, 1.86, 1.38, and the lowest values of 0.32, 0.27, 0.31, 0.25 were observed in the A, B, C, D sets of thawing experiments conducted on DR, respectively (Figure 1b). Except for the C set of experiment in which the highest CF_{DOC} value for WR was slightly lower than that for DR, all the highest CF_{DOC} values for WR in A∼D sets of thawing experiments were significantly higher than the corresponding highest values for DR ($P < 0.05$) (Figure 1), suggesting that the higher DOC concentration in ice was, the higher degree of enrichments of DOM within the first melt water fraction was.

As shown in Figure 1, although with different DOM origins (wastewater-derived DOM vs. naturally occurring DOM), for both WR and DR, the CF_{DOC} curve in B changed more gently as compared with that in A. Meanwhile, DOM was found to be released more uniformly over the entire melt period in D, in comparison with C. The results implied that with the same thawing temperature in freeze-thaw treatments, the higher the freezing temperature was, the stronger the concentration effect of DOM observed during the initial melting period was. That is because in the process of water freezing, the higher the freezing temperature is, the steadier the process would be [30]. In such situation, DOM was not incorporated within the ice lattice but exists in the interspace of ice crystal. Accordingly, in the process of melting, the

DOM existing in the interspace of ice crystal is likely to be released at the initial melting stage and the lower the freezing temperature is, the faster the ice crystal would grow making the stability of solid−liquid interface declining with it and an increase in the DOM entrainment of the ice crystal [31]. DOM in ice crystals was released into water only after ice melts in such conditions, which led to a more uniform elution behavior of DOM during ice melting. Similarly, it was found that with the same freezing temperature in freeze-thaw treatments, DOM was more likely to be eluted from ice during the initial melt period at relatively lower thawing temperatures. Based the results, regardless of the DOM origin, both the freezing and thawing temperatures were important factors influencing the elution behavior of DOM during ice melting.

Although with different shape of ice block (long and thin cylinder vs. short and thick cuboid), for both WR and DR, the CF_{DOC} values in A and E sets of thawing experiments were close and overlapped at several points during the whole melt process of ice (Figure 1). The results suggested that the shape of ice block had an insignificant effect on the elution behavior of DOC during ice melting.

In the A∼E experiments, thermal insulation materials were not applied to the containers. The containers were put in the refrigerator directly to freeze. In this case, cold energy could be transferred from the walls of the containers to the water samples. The heat transfer area was larger, and the inner walls of the containers could be taken as the cooling surface. The whole water sample entered into the supercooling status rapidly within a short time, and the ice crystal generated along the cooling surface, and the water sample froze from outside to inside. In this case, icing was an outside-in process, and it was also a water-purifying process. Thus as the impurity in water, DOM was rejected from the ice lattice when water froze into ice, and it was mainly wrapped in the innermost layer of ice after total freeze. In the F experiment, polystyrene insulations were applied at bottom and outer surface of the containers so that cold energy could only transferred from top to bottom and the water sample crystallized gradually from top to bottom. Pollutants present in the water sample were rejected from the ice phase and accumulated in the remaining liquid phase during water freezing. Therefore, most of DOM existed in the bottom layer of ice. Similarly, in the A∼E experiments, the melting process of ice was from outside to inside, and in the F experiment, it was from top to bottom. Although with different freezing and thawing manner, the elution behavior of DOM during ice melting observed in the F set of thawing experiments was similar to that in the A∼E sets of thawing experiments; DOM

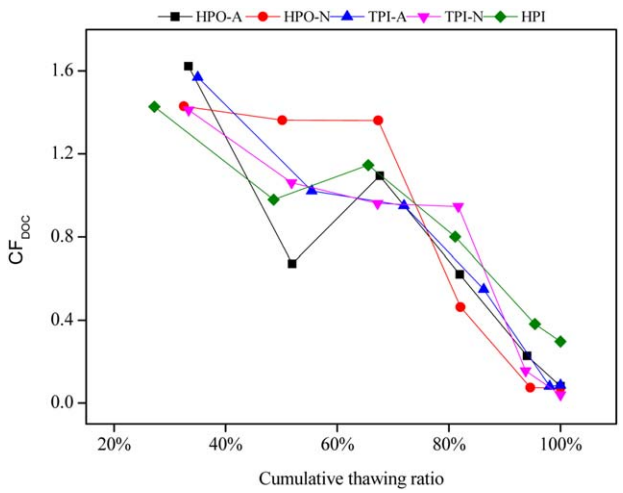

Figure 2. CF_{DOC} for five DOM fractions isolated from WR as a function of cumulative thawing ratio during ice melting. [Color figure can be viewed in the online issue, which is available at **wileyonlinelibrary.com**.]

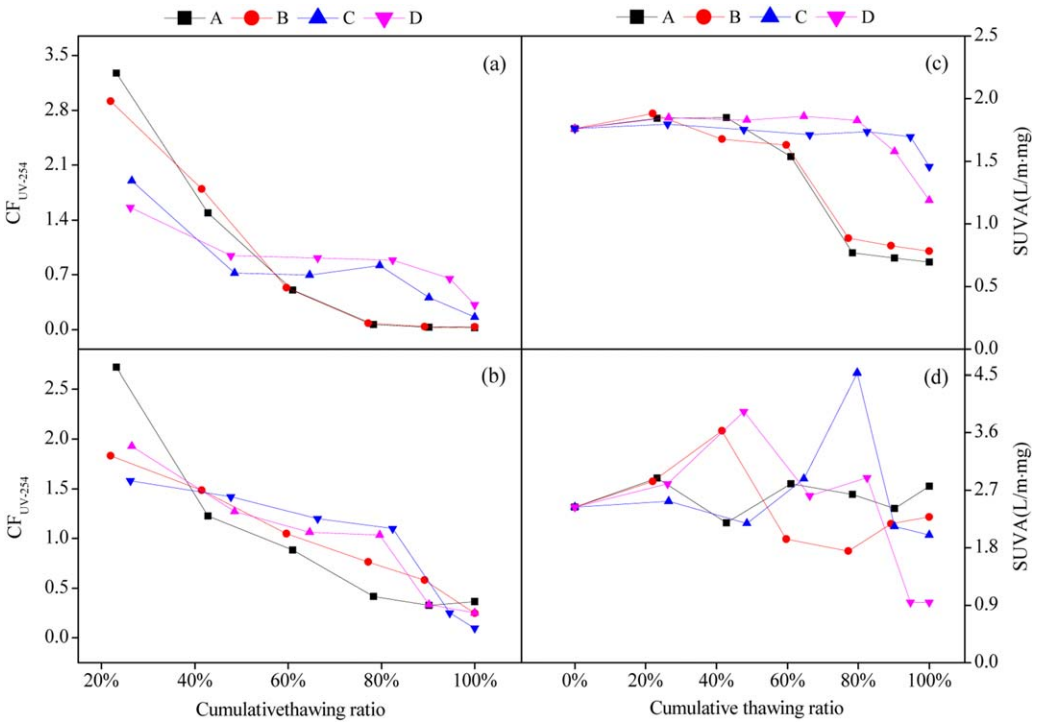

Figure 3. CF_{UV-254} for (a) WR and (b) DR and SUVA for (c) WR and (d) DR as a function of cumulative thawing ratio during ice melting. [Color figure can be viewed in the online issue, which is available at **wileyonlinelibrary.com**.]

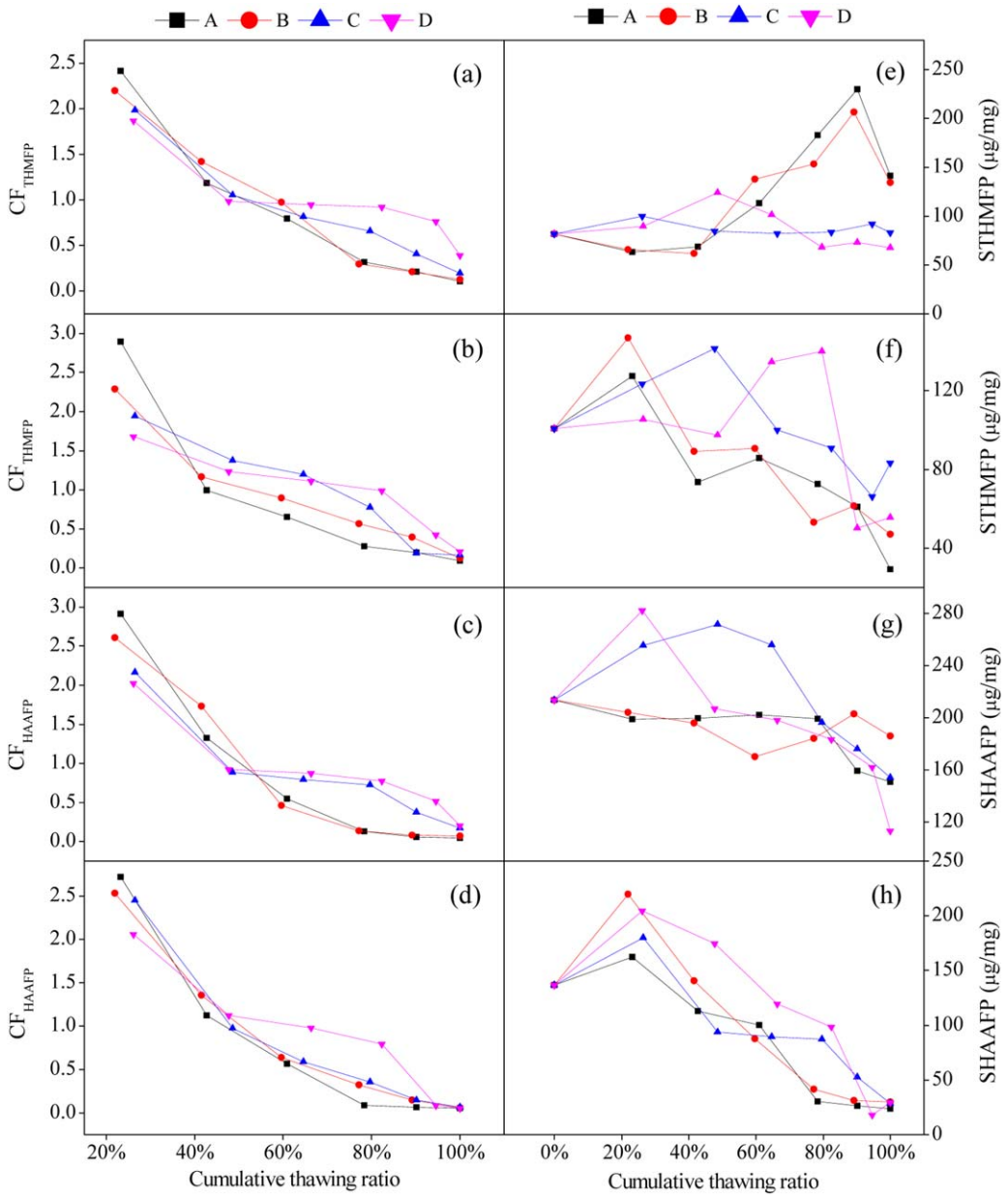

Figure 4. CF_{THMFP} for (a) WR and (b) DR, CF_{HAAFP} for (c) WR and (d) DR, STHMFP for (e) WR and (f) DR, and SHAAFP for (g) WR and (h) DR as a function of cumulative thawing ratio during ice melting. [Color figure can be viewed in the online issue, which is available at **wileyonlinelibrary.com**.]

in ice was discharged in greatly elevated concentrations at an early stage of melting, and the release of DOM was very low at the end of the melt period (Figure 1). However, a significantly higher degree of enrichments of DOM within the first melt water fraction was observed in the F set of thawing experiments, as compared with the A set of thawing experiments ($p < 0.05$) (Figure 1). Because in the A experiment, the heat transfer area of the containers was larger, the conduction velocity of heat energy was faster, and the amount of melt ice crystal at the initial melting stage was more, which weakened the concentration effect of DOM occurred during the initial melting period.

The CF values of five DOM fractions during the melting of ice were plotted as a function of cumulative thawing ratio in Figure 2. The changing trend of CF_{DOC} for the five fractions with increasing cumulative thawing ratio were similar to that for the bulk DOM which was not subject to DOM fractionation treatments shown in Figure 1, that is, the highest CF_{DOC} values occurred in the first melt water sample and the lowest CF_{DOC} values were found in the last melt water sample obtained during the melt process of ice. The CF_{DOC} values for the first melt water sample of HPO-A, HPO-N, TPI-A, TPI-N, and HPI were 1.62, 1.43, 1.57, 1.41, and 1.42, respectively. Although with the same DOC concentration of the original feed water in freeze-thaw treatments, the CF_{DOC} values for the first melt water sample of HPO-A and TPI-A were significantly higher than those for HPO-N, TPI-N, and HPI ($p < 0.05$). This suggested that the two acid fractions (i.e., HPO-A and TPI-A) were eluted earlier than the other three fractions during ice melting. Meyer and Wania [4] believed that chromatographic effects play an important role in controlling the elution order for organic chemicals, because of their wide variation in water/ice surface partitioning, and the partitioning properties of organic chemicals may

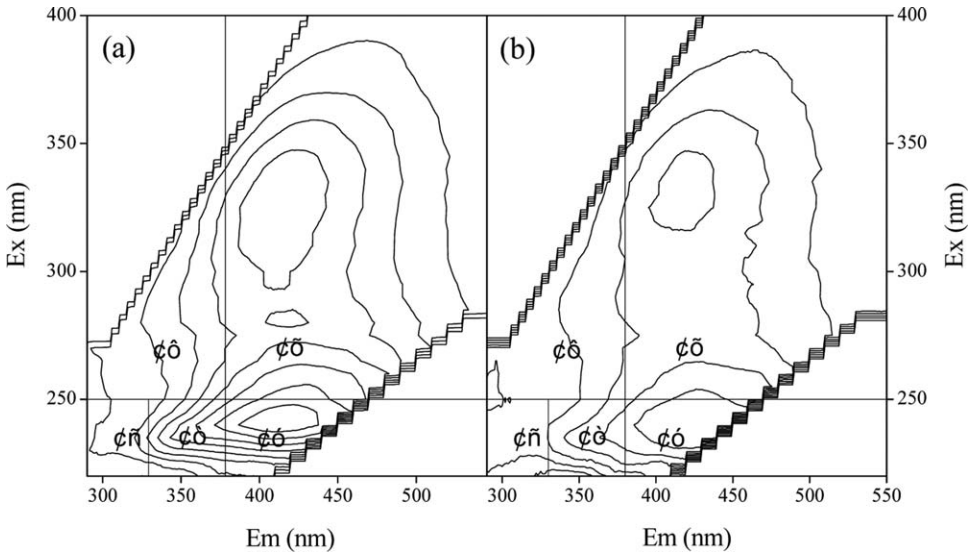

Figure 5. Fluorescence spectra for the original water samples of (a) WR and (b) DR before freeze-thaw treatments.

determine their elution order during early snowmelt. Based on the results, HPO-A and TPI-A had higher water/ice partition coefficient than the other three fractions, and they became dissolved more easily in the melt water at an early stage of melting.

Moreover, it was also noticed that the CF_{DOC} values for the first melt water sample of the five fractions fractionated from WR were all significantly lower than that for the bulk DOM of WR ($P < 0.05$), which could be attributed the their lower DOC concentrations as compared with the bulk DOM (2.5 mg/L vs. 7.2 mg/L). This again confirmed that DOC concentration had significant influence on the elution behavior of DOM during ice melting.

Release of UV-254

UV-254 is mainly caused by electro-rich sites, such as aromatic functional groups and double-bonded C groups in the DOM molecule, and is generally reflects the aromatic C═C contents [32].

Similar to the bulk DOM represented by DOC, UV-absorbing DOM were highly enriched in the first melt water fractions during ice melting, as indicated by the highest CF_{UV-254} values for both WR and DR in A∼D which all occurred in the first melt water sample (Figures 3a and 3b). Furthermore, the effect of freezing and thawing temperatures on the elution behavior of UV-254 were also similar to that on DOC; with higher freezing temperature (−15°C) and lower thawing temperature (5°C), the concentration effect of UV-254 observed during the initial melting period was stronger, whereas with lower freezing temperature (−25°C) and higher thawing temperature (15°C), UV-254 was released more uniformly over the entire melt period.

SUVA is obtained by dividing the UV-254 with its DOC, which can indicate the aromaticity of the DOM samples [33]. As shown in Figures 3c and 3d, WR and DR had SUVA values of 1.76 and 2.43 L/(m·mg), respectively, which was consistent with the previous findings that wastewater-derived DOM does not tend to be highly aromatic, although it tends to have much DOC concentrations than most surface water used as drinking water supplies [34]. The SUVA values in the melt water of WR in A∼D changed gently during the early melt process of ice (before cumulative thawing ratio of 60.0∼66.3%), and then decreased during the subsequent melting. The degree of decreases in SUVA in A and B was significantly higher than that in C and D, which implied that DOM with low aromaticity in WR was more likely to be enriched in the late melt water samples at higher thawing temperatures. On the other hand, The SUVA of DR increased slightly during the initial melting of ice. The highest SUVA values of DR in A∼D was observed in the melt water samples corresponding to cumulative thawing ratio of 41.5∼82.4%, suggesting that DOM with high aromaticity in DR was more likely to release from the ice at intermediate stage of melting. Moreover, it was also found that, for WR, DOM released from the ice formed at lower freezing temperatures at late stage of melting was generally more aromatic than that at higher freezing temperatures. However, the opposite trend was observed in DR. The results suggested that the effect of the aromaticity of DOM on its elution behavior, as well as effects of freezing and/or thawing temperatures on the changes in SUVA of DOM during ice melting, were water specific.

Release of THMFP and HAAFP

THMFP and HAAFP are often the terms employed to indicate the amount of THMs and HAAs that could be produced during the chlorination process, and could indirectly represent the amount of trihalomethane (THM) and haloacetronitrile (HAA) precursors in water samples [13,35,36].

THMFP and HAAFP of melt water samples were plotted as a function of cumulative thawing ratio in Figure 4. Both CF_{THMFP} and CF_{HAAFP} for both WR and DR in A∼D gradually decreased with increasing cumulative thawing ratio, indicating preferential elution of THM and HAA precursors with the early melt water fractions during ice melting. As a consequence, 38.8∼63.0% and 54.0∼64.3% of THM and HAA precursors were released with the first 21.9∼26.5% % melt water, respectively.

As shown in Figure 4a, the highest CF_{THMFP} values for WR in A, B, C, and D were 2.41, 2.20, 1.98, and 1.87, respectively, which increased by −22.87%, −19.47%, 9.50%, and 22.01% compared with the corresponding highest CF_{DOC} values, respectively. Meanwhile, the highest CF_{THMFP} values for DR in A, B, C, and D were 1.26, 1.45, 1.04, and 1.22 times the corresponding highest CF_{DOC} values, respectively (Figure 4b). Base on the results, the effect of freezing and/or thawing temperature on the elution order of THM precursors vs. the bulk DOM was complex and not a single influence trend.

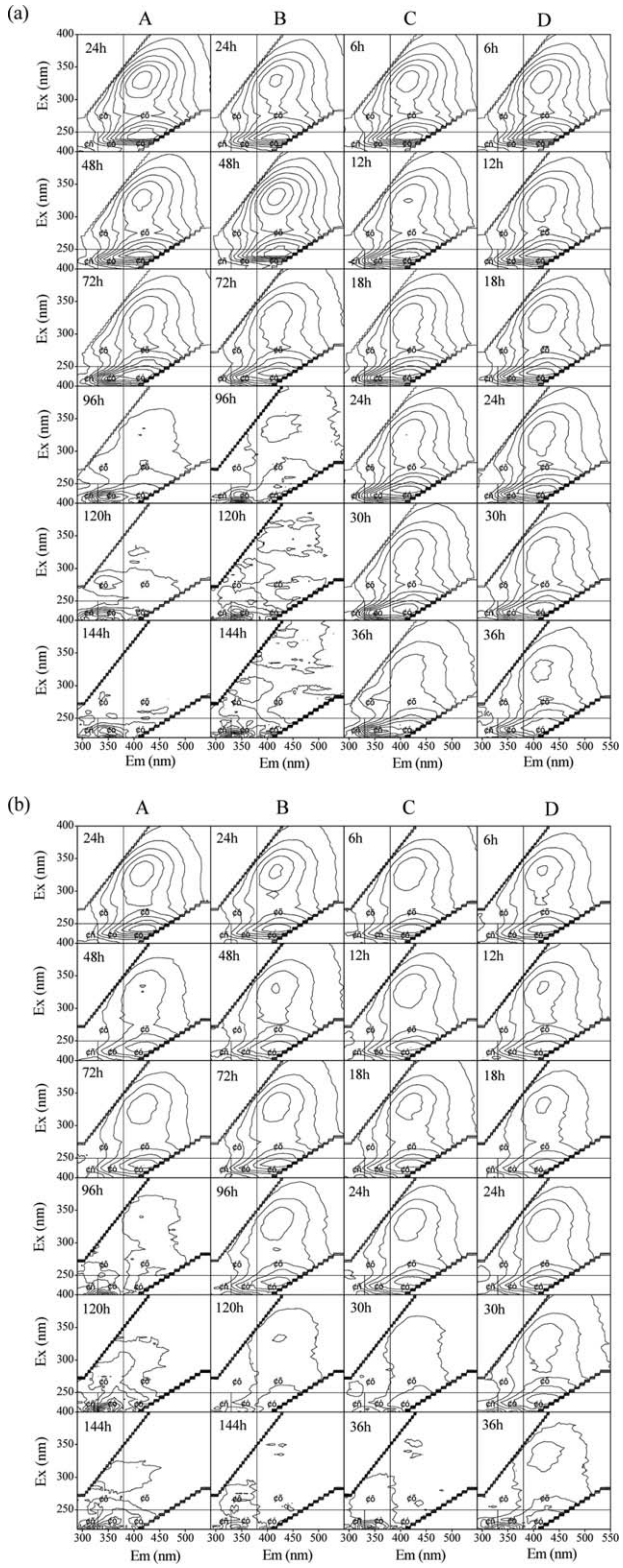

Figure 6. Fluorescence spectra for melt water samples of (a) WR and (b) DR during ice melting.

The highest CF_{HAAFP} values observed in A, B, C, and D were 2.91, 2.61, 2.12, and 2.02 for WR, and 2.72, 2.53, 2.45, 2.06 for DR, respectively (Figures 4c and 4d). Except for WR in A and B, the highest CF_{HAAFP} values for both WR and DR in A∼D were all significantly higher than the corresponding highest CF_{DOC} values ($p < 0.05$), suggesting that HAA precursors were preferentially released during the initial melting of ice as compared with the bulk DOM at higher thawing temperature (15°C) while the elution order of HAA precursors vs. the bulk DOM at lower thawing temperature (5°C) was water specific. Moreover, the ratio between the highest and lowest CF_{HAAFP} values of WR and DR in A, B, C, and D were observed to be 67.77, 38.58, 12.62, and 9.92 for WR, and 49.00, 43.59, 38.59, and 38.36 for DR, respectively, which were all significantly higher than the corresponding ratio between the highest and lowest CF_{THMFP} values (22.91, 17.26, 10.07, 4.77 for WR in A, B, C, D, respectively and 30.96, 18.50, 11.53, 8.12 for DR in A, B, C, D, respectively) ($P < 0.05$). The results implied that HAA precursors were more strongly enriched in the early melt water samples than THM precursors during ice melting.

Because THMFP is dependent upon DOC concentration, the reactivity of DOC is also reported in terms of specific THMFP (STHMFP), that is, micrograms of THMFP formed per milligram of DOC precursor material in the water (μg/mg). Similarly, specific HAAFP (SHAAFP) represents the reactivity of DOC towards chlorine and formation of HAAs. The STHMFP and SHAAFP for melt water samples of WR and DR as a function of cumulative thawing ratio were shown in Figures 4e–4h. STHMFP of WR in C and D both characterized by higher thawing freezing temperatures, showed relatively lower variation rates of −17.1∼51.8% and 0.9∼22.2% during ice melting respectively, while STHMFP in A and B both characterized by lower thawing freezing temperatures, decreased slightly at the beginning of the melt and increased significantly at late stage of melting, with relatively higher variation rates of −22.8∼181.6% and −24.5∼152.7%, respectively. On the other hand, SHAAFP for melt water samples of WR in A and B decreased by 5.3∼29.4% and 4.4∼20.3% over the entire melt period, respectively, whereas that in C and D increased by as high as 27.3% and 32.3% at early stage of melting, respectively. For DR, both STHMFP and HAAFP increased significantly at the beginning of the melt and decreased significantly at late stage of melting. The effect of freezing and/or thawing temperatures on changes in the chlorine reactivity of DOC during ice melting was complex and it was difficult to obtain a general influence trend based on the results.

Release of Fluorescent Materials

The EEM spectra were divided into five regions which represented specific components of DOM. The five regions were as follows: Regions I(Ex: 220∼250 nm/Em: 290∼330 nm) and II (Ex: 220∼250 nm/Em: 330∼380 nm) recognized as belonging to aromatic protein-like fluorescence, Region III (Ex: 220∼250 nm/Em: 380∼550 nm) associated with fulvic acid-like fluorescence, Region IV (Ex: 250∼400 nm/Em: 290∼380 nm) related to soluble microbial byproduct-like (SMP-like) florescence, and Region V (Ex: 250∼400 nm/Em: 380∼550 nm) assigned to humic acid-like fluorescence [17]. Traditionally, fulvic acid- and humic acid-like fluorescence have been associated with humic-like substances, and aromatic protein-like and SMP-like fluorescence have usually been recognized as belonging to protein-like materials. Chen *et al.* [17] proposed that integration beneath EEMs within selected regions represents the cumulative fluorescence response of DOM with similar properties. Important parameters in FRI were: (a) normalized region-specific EEM volume ($\Phi_{i,n}$), obtained by normalizing the volume beneath region "*i*" of the EEM to the fractional projected excitation-emission area; (b) cumulative EEM volume ($\Phi_{T,n}$), equal to the sum of $\Phi_{I,n} \sim \Phi_{V,n}$. The $\Phi_{i,n}$ and $\Phi_{T,n}$ values of a sample represent the amount of the fluorescent materials responsible for the fluorescence in region "*i*" of the EEM and all the fluorescent materials contained in this sample.

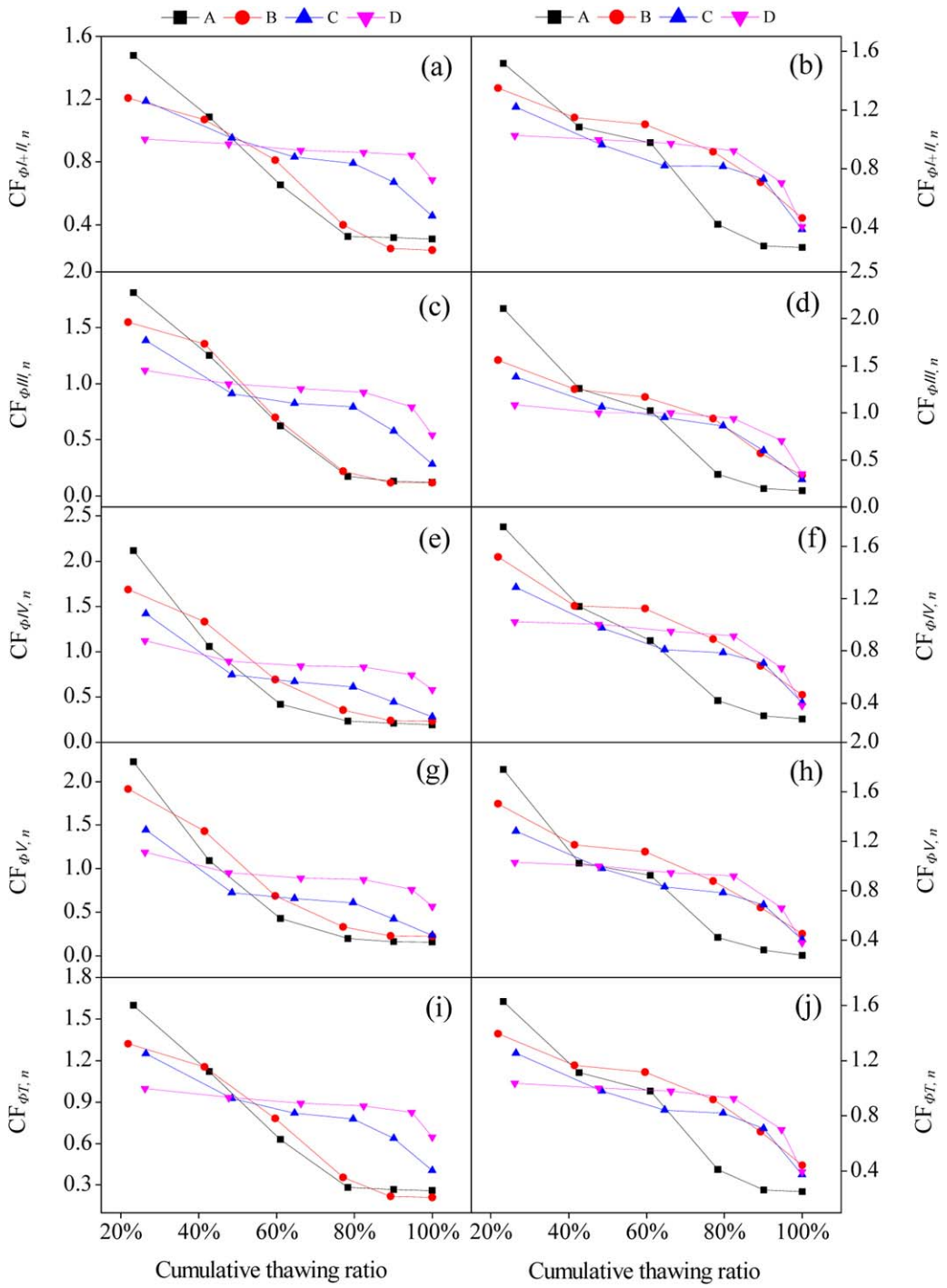

Figure 7. $CF_{\Phi I+II,\,n}$ for (a) WR and (b) DR, $CF_{\Phi III,\,n}$ for (c) WR and (d) DR, $CF_{\Phi IV,\,n}$ for (e) WR and (f) DR, $CF_{\Phi V,\,n}$ for (g) WR and (h) DR, and $CF_{\Phi T,\,n}$ for (i) WR and (j) DR as a function of cumulative thawing ratio during ice melting. [Color figure can be viewed in the online issue, which is available at **wileyonlinelibrary.com**.]

As shown in Figure 5, both WR and DR before freeze-thaw treatments were dominated by fulvic acid-like fluorescence and aromatic protein-like fluorescence in RegionsII, with WR exhibiting higher stronger fluorescence than DR.

The fluorescence spectra, and the $\Phi_{i,\,n}$ and $\Phi_{T,\,n}$ values of melt water samples of WR and DR during thawing experiments were shown in Figures 6 and 7, respectively. The sum of $\Phi_{I,n}$ and $\Phi_{II,n}$ was designated as $\Phi_{I+II,n}$ to represent the cumulative aromatic protein-like fluorescence in this study.

The fluorescent materials were released from the ice with early melt water, and were enriched in early melt water fractions, as indicated by the decreasing trend of $CF_{\Phi T,\,n}$ values of both WR and DR with increasing cumulative thawing ratio (Figures 7i and 7j). For both WR and DR, the $CF_{\Phi T,\,n}$ values in B decreased more smoothly with increasing cumulative thawing ratio, as compared with that in A, and the $CF_{\Phi T,\,n}$ curve in D changed more gently than that in C, suggesting that, regardless of the DOM origin, the fluorescent materials

were more strongly enriched in the early melt water samples at higher freezing temperatures, even at the same thawing temperatures. Meanwhile, it was found that with the same freezing temperatures at which the ice was formed, the degree of enrichments of fluorescent materials in both WR and DR within the first melt water fraction was higher at low thawing temperatures, by comparing the $CF_{\Phi T,\ n}$ curve in A to that in C, and the $CF_{\Phi T,\ n}$ curve in B to that in D. As shown in Figure 7, the $CF_{\Phi T,\ n}$ values of WR decreased from 1.60 for the first melt water sample to 0.26 for the last melt water sample in A, from 1.32 to 0.21 in B, from 1.25 to 0.40 in C, and from 1.10 to 0.65 in D, with decreases of 83.71%, 83.97%, 67.62%, and 34.95% in A, B, C, and D, respectively. The $CF_{\Phi T,\ n}$ changes were all significantly lower than the corresponding CF_{DOC} decreases (98.05%, 97.16%, 86.86%, and 74.86% in A, B, C, and D, respectively) ($p < 0.05$). This was also observed in DR thawing experiments. Based on the results, the fluorescent materials were released more uniformly over the entire melt period, as compared with the bulk DOM.

As shown in Figure 7, for both WR and DR, $CF_{\Phi I+II,\ n} \sim CF_{\Phi V,\ n}$ all followed the same changing trend with increasing cumulative thawing ratio as $CF_{\Phi T,\ n}$, indicating the similar melt behavior of four types of fluorescent materials during the melting of ice, which were as follows: all the four types of fluorescent materials exhibited a first flush behavior during ice melting, i.e., preferential elution with the early melt water fractions; the first flush behavior of the four types of fluorescent materials was stronger at higher freezing temperatures and/or at lower thawing temperatures, whereas the four types of fluorescent materials were eluted from the ice more uniformly at lower freezing temperatures and/or at higher thawing temperatures. Moreover, it was found that the highest $CF_{\Phi I+II,\ n}$ values of both WR and DR in A$\sim$D were all significantly lower than the corresponding highest $CF_{\Phi III,\ n}$, $CF_{\Phi IV,\ n}$, and $CF_{\Phi V,\ n}$ values ($p < 0.05$) (Figure 7). Take, for example, the higher $CF_{\Phi I+II,\ n}$, $CF_{\Phi III,\ n}$, $CF_{\Phi IV,\ n}$, $CF_{\Phi V,\ n}$ values were 1.48, 1.81, 2.12, 2.23 and 1.52, 2.11, 1.75, 1.78 for WR and DR in A, respectively. The results suggested a weaker first flush behavior of aromatic protein-like fluorescent materials as compared with the other three types of fluorescent materials during the melting of ice. The highest $CF_{\Phi i,n}$ values of WR in A$\sim$D could be ranked as follows: $CF_{\Phi I+II,\ n} < CF_{\Phi III,\ n} < CF_{\Phi IV,\ n} < CF_{\Phi V,\ n}$. Although this order of $CF_{\Phi i,n}$ values of DR was also observed in D, the order of $CF_{\Phi i,n}$ values of DR in B and C was as follows: $CF_{\Phi I+II,\ n} < CF_{\Phi V,\ n} < CF_{\Phi IV,\ n} < CF_{\Phi III,\ n}$, and the order of $CF_{\Phi i,n}$ values of DR in A was found to be $CF_{\Phi I+II,\ n} < CF_{\Phi IV,\ n} < CF_{\Phi V,\ n} < CF_{\Phi III,\ n}$. Based on the results, the elution order of the four types of fluorescent materials was water specific, and the effect of freezing and/or thawing temperatures on it was complex and not a single influence trend.

CONCLUSIONS

The investigation illustrated the elution behavior of DOM from melting ice. Results showed that the bulk DOM and its five fractions, as well as UV-absorbing substances, THM and HAA precursors, and fluorescent materials in DOM were discharged in elevated concentrations at an early stage of melting. The higher DOC concentration in ice was, the higher degree of enrichments of DOM within the first melt water fraction was. With higher freezing temperature and lower thawing temperature, DOM was more strongly enriched in the early melt water samples, whereas with lower freezing temperature and higher thawing temperature, DOM was released more uniformly over the entire melt period. The effect of the aromaticity of DOM on its elution behavior, as well as effects of freezing and/or thawing temperatures on the changes in SUVA of DOM during ice melting, were water specific. HAA precursors were preferentially released during the initial melting of ice as compared with the bulk DOM at relatively high thawing temperature. HAA precursors were more strongly enriched in the early melt water samples than THM precursors during ice melting. The fluorescent materials were released more uniformly over the entire melt period, as compared with the bulk DOM.

ACKNOWLEDGMENTS

The work was supported by the National Natural Science Foundation of China (No. 21107039), the Science and Technology Research Project of Liaoning Provincial Education Department (No. L2011002), and the Science and Technology Plan Project of Liaoning Province (No. 2011230009).

LITERATURE CITED

1. Li, Z.J., Wang, X., Li, Q.S., Xu, S.G., Xu, X.Z., & Bai, Y. (2008). Study on nitrobenzene ratio in water-ice system under different conditions, Science in China Series E: Technological Sciences, 51, 2013–2020.
2. Colbeck, S.C. (1981). A simulation of the enrichment of atmospheric pollutants in snow cover runoff, Water Resources Research, 17, 1383–1388.
3. Johannessen, M., & Henriksen, A. (1978). Chemistry of snow meltwater: Changes in concentration during melting, Water Resources Research, 14, 615–619.
4. Meyer, T., & Wania, F. (2008). Organic contaminant amplification during snowmelt, Water Resources, 42, 1847–1865.
5. Ulén, B. (2003). Concentrations and transport of different forms of phosphorus during snowmelt runoff from an illite clay soil, Hydrological Processes, 17, 747–758.
6. Brimblecombe, P., Clegg, S.L., Davies, T.D., Shooter, D., & Tranter, M. (1987). Observations of the preferential loss of major ions from melting snow and laboratory ice, Water Resources, 21, 1279–1286.
7. Brimblecombe, P., Clegg, S.L., Davies, T.D., Shooter, D., & Tranter, M. (1988). The loss of halide and sulphate ions from melting ice, Water Resources, 22, 693–700.
8. Her, N., Amy, G., McKnight, D., Sohn, J., & Yoon, Y. (2003). Characterization of DOM as a function of MW by fluorescence EEM and HPLC-SEC using UVA, DOC, and fluorescence detection, Water Resources, 37, 4295–4303.
9. Leenheer, J.A., & Croué, J.P. (2003). Peer reviewed: Characterizing aquatic dissolved organic matter, Environmental Science and Technology, 37, 18A–26A.
10. Wei, Q.S., Feng, C.H., Wang, D.S., Shi, B.Y., Zhang, L.T., Wei, Q., & Tang, H.X. (2008). Seasonal variations of chemical and physical characteristics of dissolved organic matter and trihalomethane precursors in a reservoir: A case study, Journal of Hazardous Materials, 150, 257–264.
11. Wang, D.S., Zhao, Y.M., Xie, J.K., Chow, C.W.K., & Leeuwen, J.V. (2013). Characterizing DOM and removal by enhanced coagulation: A survey with typical Chinese source waters, Separation and Purification Technology, 110, 188–195.
12. Kim, H.C., & Yu, M.J. (2005). Characterization of natural organic matter in conventional water treatment processes for selection of treatment processes focused on DBPs control, Water Resources, 39, 4779–4789.
13. Ma, D.F., Gao, Y., Gao, B.Y., Wang, Y., Yue, Q.Y., & Li, Q. (2014). Impacts of powdered activated carbon addition on trihalomethane formation reactivity of dissolved organic matter in membrane bioreactor effluent, Chemosphere, 117, 338–344.
14. Rakruam, P., & Wattanachira, S. (2014). Reduction of DOM fractions and their trihalomethane formation potential in surface river water by in-line coagulation with ceramic membrane filtration, Journal of Environmental Sciences, 26, 529–536.

15. Xue, S., Zhao, Q.L., Wei, L.L., & Ren, N.Q. (2009). Behavior and characteristics of dissolved organic matter during column studies of soil aquifer treatment, Water Resources, 43, 499–507.
16. Xiao, X., Zhang, Y.J., Wang, Z.G., Jin, D., Yin, G.F., Zhao, N.J., & Liu, W.Q. (2010). Experimental studies on three-dimensional fluorescence spectral of mineral oil in ethanol, Spectroscopy and Spectral Analysis, 30, 1549–1554.
17. Chen, W., Westerhoff, P., Leenheer, J.A., & Booksh, K. (2003). Fluorescence excitation-emission matrix regional integration to quantify spectra for dissolved organic matter, Environmental Science and Technology, 37, 5701–5710.
18. Thomas, S., & Reimer, H. (1987). Transport and chemodynamics of organic micropollutants and ions during snowmelt, Nordic Hydrology, 18, 259–278.
19. Simmleit, N., & Herrmann, R. (1987). The behavior of hydrophobic, organic micropollutants in different karst water systems, Water Air and Soil Pollution, 34, 79–95.
20. Cragin, J.H., Hewitt, A.D., & Colbeck, S.C. (1996). Grain-scale mechanisms influencing the elution of ions from snow, Atmospheric Environment, 30, 119–127.
21. Harrington, R.F., Bales, R.C., & Wagnon, P. (1996). Variability of meltwater and solute fluxes from homogeneous melting snow at the laboratory scale, Hydrological Processes, 10, 945–953.
22. Meyer, T., Lei, Y.D., & Wania, F. (2006). Measuring the release of organic contaminants from melting snow under controlled conditions, Environmental Science and Technology, 40, 3320–3326.
23. Nakagawa, K., Nagahama, H., Maebashi, S., & Maeda, K. (2010). Usefulness of solute elution from frozen matrix for freeze-concentration technique, Chemical Engineering Research and Design, 88, 718–724.
24. Kammerer, P.A., & Lee, G.F. (1969). Freeze concentration of organic compounds in dilute aqueous solutions, Environmental Science and Technology, 3, 276–278.
25. Bhatnagar, B.S., Cardon, S., Pikal, M.J., & Bogner, R.H. (2005). Reliable determination of freeze-concentration using DSC, Thermochimica Acta, 425, 149–163.
26. Sánchez, J., Ruiz, Y., Raventós, M., Auleda, J., & Hernández, E. (2010). Progressive freeze concentration of orange juice in a pilot plant falling film, Innovative Food Science and Emerging Technologies, 11, 644–651.
27. Knight, C.A. (1979). Observations of the morphology of melting snow, Journal of Atmospheric Science, 36, 1123–1130.
28. Xue, S., Wen, Y., Hui, X.J., Zhang, L.N., Zhang, Z.H., Wang, J., & Zhang, Y. (2015). The migration and transformation of dissolved organic matter during the freezing processes of water, Journal of Environmental Science, 27, 168–178.
29. Nakagawa, K., Maebashi, S., & Maeda, K. (2009). Concentration of aqueous dye solution by freezing and thawing, The Canadian Journal of Chemical Engineering, 87, 779–787.
30. Belén, F., Benedetti, S., Sánchez, J., Hernández, E., Auleda, J.M., Prudêncio, E.S., Petrusb, J.C.C., & Raventós, M. (2013). Behavior of functional compounds during freeze concentration of tofu whey, Journal of Food Engineering, 116, 681–688.
31. Belén, F., Sánchez, J., Hernández, E., Auleda, J.M., & Raventós, M. (2012). One option for the management of wastewater from tofu production: Freeze concentration in a falling-film system, Journal of Food Engineering, 110, 364–373.
32. Yang, Y., Lohwacharin, J., & Takizawa, S. (2014). Hybrid ferrihydrite-MF/UF membrane filtration for the simultaneous removal of dissolved organic matter and phosphate, Water Resources, 65, 177–185.
33. Pifer, A.D., & Fairey, J.L. (2012). Improving on SUVA 254 using fluorescence-PARAFAC analysis and asymmetric flow-field flow fractionation for assessing disinfection byproduct formation and control, Water Resources, 46, 2927–2936.
34. Sirivedhin, T., & Gray, K.A. (2005). 2. Comparison of the disinfection by-product formation potentials between a wastewater effluent and surface waters, Water Resources, 39, 1025–1036.
35. Iriarte-Velasco, U., Álvarez-Uriarte, J.I., & González-Velasco, J.R. (2007). Removal and structural changes in natural organic matter in a Spanish water treatment plant using nascent chlorine, Separation and Purification Technology, 57, 152–160.
36. Wu, M.N., Wang, X.C., & Ma, X.Y. (2013). Characteristics of THMFP increase in secondary effluent and its potential toxicity, Journal of Hazardous Materials, 261, 325–331.